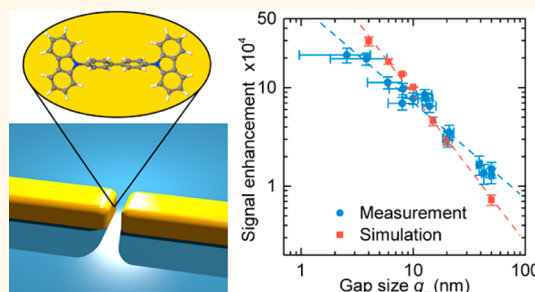


Surface-Enhanced Infrared Spectroscopy Using Nanometer-Sized Gaps

Christian Huck,[†] Frank Neubrech,^{†,‡} Jochen Vogt,[†] Andrea Toma,[§] David Gerbert,[†] Julia Katzmann,[§] Thomas Härtling,[§] and Annemarie Pucci^{†,§,*}

[†]Kirchhoff Institute for Physics, University of Heidelberg, Im Neuenheimer Feld 227, 69120 Heidelberg, Germany, [‡]4th Physics Institute and Research Center SCoPE, University of Stuttgart, Pfaffenwaldring 57, 70569 Stuttgart, Germany, [§]Fraunhofer Institute for Ceramic Technologies and Systems, Materials Diagnostics, Maria-Reiche-Str. 2, 01109 Dresden, Germany, [§]Istituto Italiano di Tecnologia, Via Morego 30, 16163 Genova, Italy, and ^{||}Centre for Advanced Materials, University of Heidelberg, Im Neuenheimer Feld 227, 69120 Heidelberg, Germany

ABSTRACT We report on the near-field coupling of individual gold nanoantennas arranged in tip-to-tip dimer configuration, leading to strong electromagnetic field enhancements in the infrared, which is of great interest for sensing applications such as surface-enhanced infrared spectroscopy. We quantitatively evaluated the enhancement of vibrational excitations of a 5 nm thick test layer of 4,4'-bis(*N*-carbazolyl)-1,1'-biphenyl as a function of different gap sizes. The dimers with the smallest gaps under investigation (~ 3 nm) lead to more than 1 order of magnitude higher signal enhancement with respect to gaps of 50 nm width. The comparison of experimental data and finite-difference time-domain simulations reveals a nonperfect filling of the gaps with sizes below 10 nm, which means that morphological information on the nanoscale is obtained additionally to chemical information.



KEYWORDS: plasmonic · nanogaps · surface-enhanced infrared absorption · SEIRA · optical nanoantenna · infrared

Metal nanoparticles attract much interest in the field of nano-optics because it is possible to excite plasmon polaritons within the particles, which in turn can couple to other excitations with similar energies. Hence, these nanostructures can be exploited to increase the sensitivity of spectroscopic methods by placing a molecular species on surface areas exhibiting enhanced electromagnetic fields. The application of such “hot spots” induced by nanostructures with various geometries was shown many times, for example, for surface-enhanced fluorescence,^{1,2} surface-enhanced infrared absorption (SEIRA),^{3–5} and surface-enhanced Raman spectroscopy (SERS).^{6–9} Using rod-shaped nanoparticles covered with probe molecules, SEIRA enhancement factors of up to 5 orders of magnitude have been reported, which corresponds to an attomolar detection sensitivity.¹⁰ One possibility to further push the detection limit is the use of nanostructures arranged in arrays where their far-field

coupling leads to the collective excitation of the ensemble.¹¹ Another option is nanoparticles with near-field interaction across a nanometer-sized gap.^{12,13} Theoretical calculations show that the intensity of the electromagnetic field in a gap of less than 10 nm can be several orders of magnitude higher than those of single structures.^{14–16} These findings, hence, promise to drastically improve the sensitivity of surface-enhanced sensing applications, where the signal intensity scales with the intensity (to the power of one or two) of the near-field at the metal surface.^{15,17–19} This idea has already been applied to other sensing methods, such as SERS,^{20–25} surface-enhanced fluorescence,² and also to SEIRA.^{17,26}

Therefore, the controlled preparation of such gaps in the sub-10 nm regime is highly desired but still challenging, especially in the IR, where structures with dimensions in the micrometer range must be combined with nanometer-sized gaps. Different approaches have been applied to address this

* Address correspondence to pucci@kip.uni-heidelberg.de.

Received for review February 14, 2014 and accepted April 11, 2014.

Published online April 11, 2014
10.1021/nn500903v

© 2014 American Chemical Society

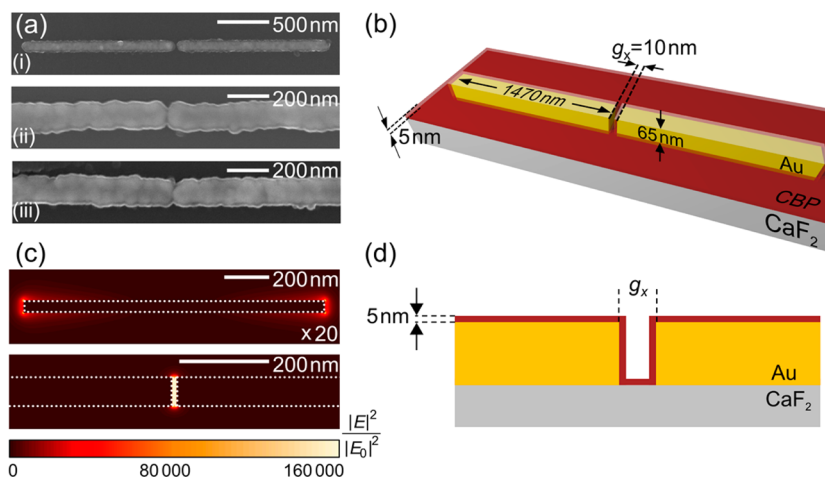


Figure 1. (a) SEM image of typical nanoantenna dimers with photochemically narrowed gaps on a CaF₂ substrate. (b) Sketch of the geometry with a 10 nm gap and a 5 nm thick layer of CBP molecules used for numerical calculations. (c) FDTD simulated near-field intensity distribution of a single antenna and an antenna dimer (10 nm gap) at the respective resonance frequencies. The intensity of the single antenna has been multiplied by a factor of 20. A plane wave was considered as the incident electromagnetic field. The near-field maps were calculated in a plane 32.5 nm above the CaF₂ substrate. The white dotted lines represent the contours of the structures. (d) CBP coverage inside the gap region as assumed for FDTD calculations.

TABLE 1. Assignment of Selected CBP Absorption Bands^a

frequency (cm ⁻¹)	mode assignment
1230	$\delta(C-H)_c$
1317	$\delta(C-H)$
1335	$\delta(C-H)$, $\nu(C-N)$, $\nu(C-C)$
1360	$\delta(C-H)$, $\nu(C-N)$
1450	$\delta(C-H)_c$
1479	$\delta(C-H)_c$
1504	$\delta(C-H)_b$, $\nu(C-N)$
1603	$\nu(C-O)_b$, $\delta(C-H)_b$
1624	$\delta(C-C)$, $\delta(C-H)$

^a δ and ν refer to deformation and stretching modes, respectively; *c* and *b* indicate a dominant localization on the carbazole groups or biphenyl, respectively.

problem, but difficulties remain: For instance, the preparation by electron beam lithography (EBL) is limited by the proximity effect, and the cutting of nanoantennas with focused ion beams is delicate because the remaining material may close the gap.²⁷ In a previous contribution, we demonstrated the fabrication of nanoscale gaps by combining EBL and subsequent photochemical metal deposition (PCMD).¹³ Nanogaps down to 3 nm were successfully prepared as confirmed by finite-difference time-domain (FDTD) simulations.

In this contribution, we systematically investigate the benefit of nanoscale gaps for SEIRA. In order to evaluate the SEIRA activity, single antennas and dimers were covered with a 5 nm thick test layer of 4,4'-bis(*N*-carbazolyl)-1,1'-biphenyl (CBP) under ultrahigh vacuum conditions (see Methods). Subsequent SEIRA measurements of single and dimer structures were performed using synchrotron radiation (see Methods). The recorded spectra were painstakingly baseline-corrected to allow the precise quantitative evaluation of vibrational

signals. We discuss the development of both the signal intensity and the CBP-layer-induced plasmon shift with decreasing gap size and compare the results with FDTD simulations.

RESULTS AND DISCUSSION

Gold nanoantennas were prepared by means of EBL and subsequently enlarged *via* PCMD. By changing the PCMD parameters, different gaps sizes ranging from 3 to 50 nm were realized, as shown in Figure 1a. The gold nanoantennas were covered with a CBP layer of 5 nm average thickness. CBP features various infrared active vibrational modes (see a selection of prominent ones in Table 1). The assignment of frequencies to CBP vibrations originates from the comparison to intensities and frequencies from density function theory calculations.²⁸

Typical IR relative transmittance spectra of a dimer with a gap of 50 nm (green), a gap of 8 nm (red), and a merged dimer (blue) covered with CBP are shown in Figure 2. Their resonance frequencies (minimum of transmittance) shift to lower energies due to the decreasing gap size and thus the increasing attraction forces between the charge carriers across the gap which reduce the restoring forces driving the charge oscillations. The two important consequences for SEIRA are the increased field enhancement in the gap and its spectral broadening.^{16,29} Therefore, almost all vibrational modes of CBP in a rather broad interval can be clearly seen in the case of few nanometer small gaps since the signal intensity (and the line shape) of the various vibrational modes is closely related to the tuning to the plasmonic resonance spectrum.³⁰ It is known from literature that the highest signal intensity is achieved if the vibrational frequency matches the

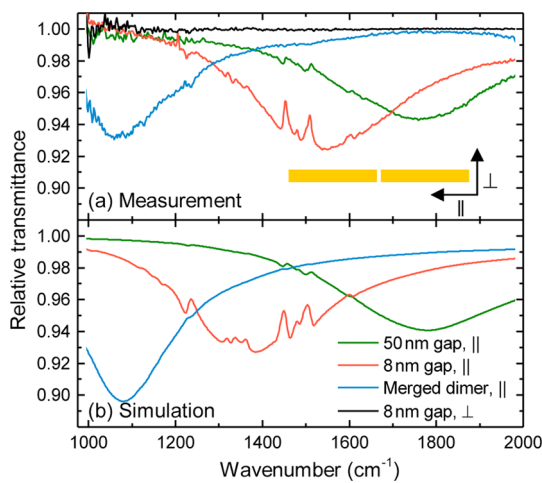


Figure 2. Selection of experimental relative transmittance spectra (a) and simulated (see Figure 1d) relative transmittance (b) of single nanoantenna dimers with different gap sizes, covered with 5 nm CBP. The symbols \parallel and \perp indicate the longitudinal and the transverse polarization, respectively, with respect to the long antenna axis. Differences between the measurements and the simulations are discussed in the text.

maximum near-field intensity³¹ and thus is slightly red-shifted compared to the far-field resonance frequency.^{32–34} To compare different dimers, it is thus necessary to take into account the detuning between the vibrational frequency and the near-field resonance frequency of the nanostructures. In the case of the dimer with the smallest gap, which features the highest vibrational signals, nine CBP modes in a broadband range of around 400 cm^{-1} ($1230\text{--}1624\text{ cm}^{-1}$) are observed.²⁸ This broadband detection of vibrational modes is essential for safe molecular identification and characterization of any modifications. The spectrum of the dimer with larger gap size, however, contains only the strongest vibrational modes, and the merged dimer does not show any clear signal due to both lower field enhancement because of the missing gap and a much larger detuning between the vibrational and the plasmonic resonance.

To confirm our measurement results, FDTD simulations were carried out using the total field scattered field (TFSF) approach. The antennas were described as cuboid-shaped objects with a geometry shown in Figure 1b. CBP molecules were modeled as a 5 nm film covering the entire sample surface homogeneously, including the whole substrate and all side walls of the antennas (see Figure 1c,d). Initial antennas that were not photochemically treated showed dimensions $l \times w \times h = 1460 \times 60 \times 60\text{ nm}^3$ and a gap size of about 20 nm. Photochemically grown and therefore smaller gaps were taken into account in the simulation by assuming a uniform growth of the antenna dimensions in each direction leading to a final size of $2960 \times 80 \times 70\text{ nm}^3$ for the merged dimer. This assumption is a good approximation of the real geometry since

surface roughness and inhomogeneities in l , w , and h are small compared to the antenna dimensions. However, for small gaps, the surface roughness might play an important role because it can change the gap distance and induce additional hot spots.³⁵ For very small gap sizes, quantum effects such as electron tunneling can suppress the near-field enhancement³⁶ and therefore lower the intensity of SEIRA signals. These effects are neglected here since they should play a minor role for separation distances larger than 1 nm.³⁶ The simulated spectra are shown in Figure 2b. All vibrational features of CBP observed in the SEIRA experiment could be reproduced within the simulation. However, the resonance frequency and therefore also the vibrational signal line shape of the dimer with 8 nm gap are modified compared to the measurement result, indicating an imperfect filling of the gap as we will discuss later.

In order to quantitatively evaluate the vibrational signal strength, a baseline correction of the measured and the simulated spectra was performed. The baseline given by the plasmonic resonance was estimated using an adaption of the computational approach of asymmetric least-squares smoothing (AsLSS) introduced by Eilers³⁷ (see Supporting Information for further details). One advantage of this algorithm for our analysis is the possibility to exclude regions with vibrational signals. Figure 3 shows the AsLSS baseline correction for a dimer with a gap size of 8 nm. The reference spectrum was acquired from a large area of the 5 nm CBP layer on CaF_2 (top panel in Figure 3). This spectrum was also used to determine the spectral regions of CBP vibrational features, which were then excluded for the baseline matching procedure. The measured spectrum and the resulting baseline obtained from the algorithm are shown in the middle panel. Finally, the resulting baseline-corrected spectrum $T_{\text{meas}}(\omega)/T_{\text{baseline}}(\omega)$ is shown in the bottom panel. The baseline-corrected signals show a Fano-type behavior as it is known from literature.^{10,30} Depending on the match between the vibrational frequency and the resonance frequency, the line shape goes from a dip for perfect matching to an asymmetric line shape.

After the signals were baseline-corrected, the peak-to-peak values of the vibrational signals were read out from the spectra like that in the bottom panel of Figure 3. The enhancement of the vibrational bands depends not only on the gap size but also on the spectral match between the vibrational resonance and the plasmonic spectrum, that is, the tuning ratio $\beta = \omega_{\text{res}}/\omega_{\text{vib}}$ between the plasmonic resonance frequency ω_{res} and the vibrational resonance frequency ω_{vib} . Due to a shift between the near- and the far-field peak intensities, the highest enhancement is not achieved for $\beta = 1$ but for values slightly higher than 1.^{31,32,34} Looking at the vibrational modes of CBP, the dimer with the 50 nm gap features a resonance

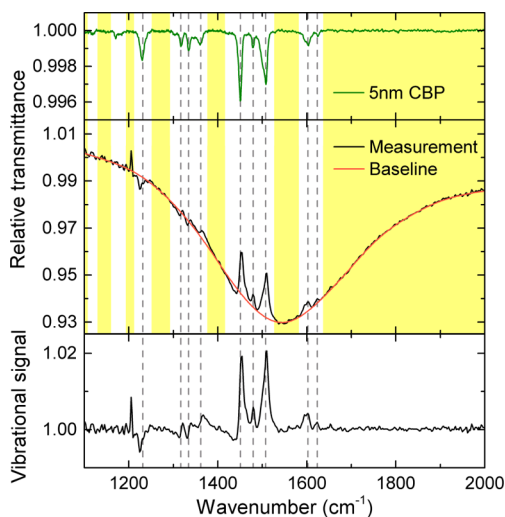


Figure 3. Iteratively estimated baseline using an AsLSS algorithm. Top panel shows the reference measurement of 5 nm CBP on a CaF_2 substrate (measurement spot size: 3 mm in diameter). Only spectral regions without vibrational features were used for baseline correction (yellow background in the top and middle panel). The middle panel displays an overlay of measured data from a dimer with an 8 nm gap and the baseline as calculated by the AsLSS algorithm. The bottom panel shows the baseline-corrected vibrational signal $T_{\text{meas}}/T_{\text{baseline}}$. The strongest vibrational modes of CBP are marked with a dashed vertical line.

frequency that is obviously at higher wavenumbers, whereas the merged dimer shows a resonance frequency that is clearly lower than the strongest CBP vibration at 1450 cm^{-1} (see Figure 2). The antenna dimer with the gap of 8 nm, however, shows a good match between its resonance frequency and the strongest vibrational mode of CBP. This results in a much higher signal for this small gap, which is induced not only by the higher near-field enhancement in the gap but also by the better tuning ratio.

In order to separate the influence of β from the influence of the gap size on the SEIRA enhancement, a second sample with a series of nanoantenna arrays with various length between 1300 and 2550 nm and thus different resonance frequencies was investigated. The same amount of CBP was evaporated on this sample, and the vibrational signals for two prominent CBP bands (1230 and 1450 cm^{-1}) were evaluated with respect to β . The resulting curve is shown in Figure S2. By fitting the model of an externally driven damped harmonic oscillator,³³ we finally end up with a correction function $C_{\text{detuning}}(\beta)$ (see Supporting Information for further information).

Furthermore, for calculating an enhancement factor, one has to assume an area A_{gap} which is covered with CBP. Because CBP was evaporated under normal incidence, the side walls of the antennas may not be homogeneously evaporated, but at room temperature, CBP molecules may diffuse on the surface and also cover the side walls. For the calculation of the

enhancement factor, ideal conditions are assumed where all the side walls are homogeneously covered with CBP. The areas taken into account for calculating the enhancement factor (EF) are the front walls of the antenna, which form the gap and the substrate surface between the two antennas (see inset of Figure S4 in the Supporting Information). In order to estimate the fraction of the enhanced CBP signal that is generated by molecules inside the gap and not by molecules outside, the near-field intensity distributions of single antennas and antenna dimers from the FDTD simulations were considered (see Figure 1c and Figure S3 in the Supporting Information). For example, the near-field intensity of a single nanoantenna and a nanoantenna dimer with a gap of 10 nm is shown in Figure 1c. The hot spots of the single antenna at the fundamental resonance are localized at both antenna apexes,⁵ but the near-field of the antenna dimer is mainly confined to the gap region. Therefore, we can safely assume that for gap sizes below 10 nm CBP molecules inside the gap dominate the signal. In order to quantitatively estimate how much the molecules inside the gap contribute to the signal, FDTD simulations with the CBP layer only in the gap region (see inset of Figure S4) have been carried out. By comparing the vibrational signal of these simulations with those shown in Figure 2, we calculate the ratio $C_{\text{gap}} = I_{\text{SEIRA,gap}}/I_{\text{SEIRA}}$ of the SEIRA signal $I_{\text{SEIRA,gap}}$ generated in the gap and the signal I_{SEIRA} generated by the whole CBP layer (see Figure S4). The fraction originating from the gap only is about 25% for very large gaps (50 nm) and increases up to 80% for gaps smaller than 10 nm. Similar values have been reported in literature.^{17,38}

The enhancement factor for the gap region corresponding to perfect tuning is calculated with the relation

$$\text{EF} = \frac{I_{\text{SEIRA}} \times C_{\text{gap}}}{I_{\text{ref}}} \times \frac{A_0}{A_{\text{CBP}}} \times C_{\text{detuning}} \quad (1)$$

where I_{SEIRA} is the signal size obtained from the baseline-corrected peak-to-peak value of the Fano-type vibrational signal (see Figure 3 and Figure S1 in the Supporting Information), I_{ref} is the reference signal (top panel of Figure 3), and A_0 is the area illuminated in the IR measurement of the antenna dimer which is given by the aperture used in the experiment ($15 \times 15 \mu\text{m}^2$).

The enhancement factor according to eq 1 in dependence of the gap size is shown in Figure 4. Each point in this figure corresponds to an individual antenna dimer for which the enhancement of the strongest CBP vibration at 1450 cm^{-1} (C–H deformation vibration) was analyzed. Both the experiment and the simulation show a strong increase of the signal enhancement with decreasing gap size, starting with approximately 10 000 for a 50 nm gap and reaching nearly 200 000 in the experiment and more than 250 000 in the simulation at a gap size of 4 nm. It is

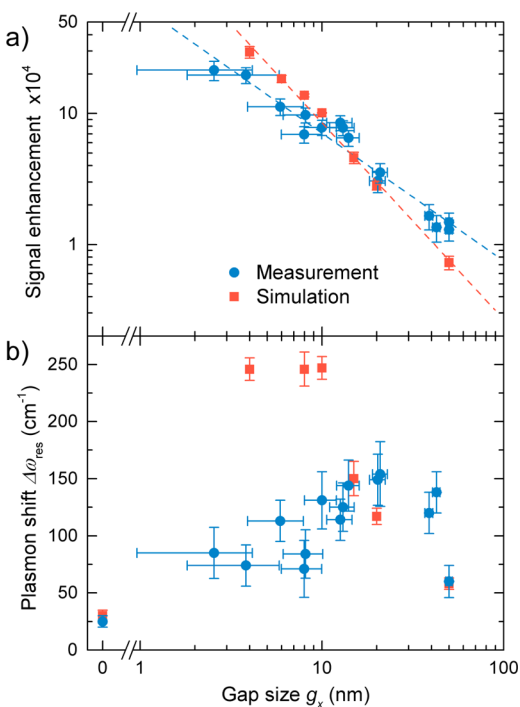


Figure 4. (a) Measured (blue) and simulated (red, model Figure 1d) signal enhancement EF of the gap region for the vibration at 1450 cm^{-1} of the CBP molecules adsorbed on nanoantenna dimers with different gap sizes g_x . The power-law $\text{EF} \propto A \times g_x^m$ was fitted to the data. (b) Shift of the plasmon resonance due to the whole CBP layer plotted versus the dimer gap size. The error for the simulations in (a) originates from the detuning correction that is based on a measurement, and in (b), they are due to uncertainties in the readout of the resonance frequency because the plasmonic spectrum is modified by the vibrational features.

important to note that these EF data represent average values for the whole CBP thickness.

Since the infrared absorption scales with the near-field intensity, the general power-law relationship $\text{EF} \propto |E|^2 = A \times g_x^m$ was fitted to the data giving a slope of $m_{\text{exp}} = -0.97 \pm 0.06$ for the measurement and $m_{\text{sim}} = -1.50 \pm 0.05$ for the numerical simulation. Both values indicate a weak power-law dependence of the electric field E on the gap size ($E \propto g_x^{-0.49}$ and $E \propto g_x^{-0.75}$, respectively), even weaker than the decay of a monopole field ($E \propto d^{-2}$ according to Coulomb's law). Similar results ($E \propto g_x^{-0.56}$) were reported in literature for surface-enhanced Raman scattering ($\text{EF} \propto |E|^4 = A \times g_x^{2m}$) from bowtie nanoantennas.²³ The deviation between the exponents m in the simulation and the experiment is related to the nonideal coverage inside the smaller gaps, which is even more obvious in the shift of the plasmon resonance.

The plasmon shift $\Delta\omega_{\text{res}}$, induced by the entire CBP layer (see Figure 4b), also shows significant differences between simulation and experiment: for large gaps, the simulations match very good to the measured data. By decreasing the gap size in the FDTD simulation, the red shift of the plasmon resonance increases until the gap size is equal to 10 nm and stays constant for smaller gaps because of complete CBP filling assumed in the FDTD model. For gaps larger than 10 nm, the gap region in the FDTD model is not totally filled with CBP: 5 nm layer is placed on each surface (see Figure 1d). Therefore, the simulated red shift stays constant when the gap is completely filled with CBP. In the measurement, however, the shift of the resonance frequency decreases if the separation between the two antennas reaches values below 10 nm (*i.e.*, below twice the CBP thickness). The smaller red shift (corroborating the lower EF) for gaps below 10 nm can be attributed to the imperfect filling of gaps of antenna dimers. The enhancement factors derived from the experiments under the assumption of perfect gap filling thus give a lower bound for the real values.

The observed deviations between simulation and experiment indicate a method of far-field monitoring on the nanoscale where the controlled filling of nanoholes is important. Due to the different thermodynamics on the nanoscale,³⁹ adsorption and diffusion parameters may deviate from such on extended planar surfaces.

SUMMARY AND CONCLUSION

We have demonstrated the broadband enhanced detection of infrared vibrational signatures of organic molecular layers on nanoantenna dimers. By decreasing the size of the gap between the two arms of the antenna dimer down to 3 nm, SEIRA enhancement factors increase by more than 1 order of magnitude in comparison to antennas separated by 50 nm. Significant deviations between experiment and FDTD simulations for totally full gaps are observed. These discrepancies can be ascribed to difficulties in homogeneously filling nanometer-sized gaps with nanometer-sized molecules. Since the narrowest gaps give the highest enhancement, it is desirable to go to these limits as close as possible in sensing applications. Monitoring of the successful filling of a gap should be possible with our approach since the SEIRA intensity and also the plasmonic shift strongly depend on the filling of the nanogap as shown in our study.

METHODS

Gold Nanoantenna Preparation. Nanoantennas and nanoantenna dimers were fabricated according to the EBL nanopatterning technique. After the substrate was cleaned in an ultrasonic bath of acetone, poly(methyl methacrylate) (PMMA) was spin-coated

on the $\text{CaF}_2(100)$ substrate at 3000 rpm. An Al layer of 10 nm thickness was thermally evaporated on the PMMA surface in order to avoid surface charging. Therefore, EBL machine (electron energy 20 keV and beam current 45 pA), equipped with a pattern generator (Raith 150-Two), was employed for the

nanostructure patterning. The Al layer was removed in a KOH solution, and then the exposed resist was developed in a conventional solution of MIBK/IPA (1:3) for 30 s. Physical vapor deposition (evaporation rate 0.3 Å/s) of 5 nm Ti as adhesion layer and 55 nm Au was performed on the sample. Finally, the unexposed resist was removed in an ultrasonic bath of acetone. In order to avoid organic residues, O₂ plasma ashing at 200 W for 60 s was carried out.

After EBL fabrication, the gap size between a typical gold antenna dimer was around 20 nm. To further decrease the distance between the two antenna arms, photochemical metal deposition was carried out on the antenna dimers. Therefore, the sample was covered with a droplet of 5 μM HAuCl₄ solution and illuminated with a Nd:YAG laser. Due to the reduction of the gold salt, gold ions were generated and accumulated on the nanoantennas, which led to a gradual growth of the nanoantennas. When we applied this approach, nanogaps with a size down to 3 nm were produced. Further details about the sample preparation and dimer characterization can be found in ref 13. For the SEM measurements, which were performed after the IR experiments, the sample was covered with a thin carbon layer. This carbon layer hampers the measurement of the antenna dimensions.

Evaporation of the CBP Film and Reference Measurement. Subsequent to the preparation and characterization of the nanoantennas, the sample was cleaned in oxygen plasma at 150 W for 10 min. Afterward, the sample was placed in an ultrahigh vacuum chamber for the evaporation of the CBP (Sigma-Aldrich, 4,4'-bis(*N*-carbazolyl)-1,1'-biphenyl, 99.9%) layer²⁸ onto the whole sample surface at room temperature. CBP forms an amorphous, almost homogeneous layer (rms <1 nm) that is stable in air for a few weeks. IR microscopy has confirmed the thickness homogeneity over an area of 3 mm in diameter.

A transmittance spectrum of the whole substrate covered with CBP was taken as the SEIRA reference. The antennas in this measurement can be neglected because they cover less than 0.00001 of the total measurement area. The reference measurement was also used to calculate the CBP layer thickness with the help of the dielectric function of CBP.²⁸ This was done using the software SCOUT⁴⁰ with a resultant layer thickness of 4.4 nm, which is in good agreement with the value of 5.3 nm estimated from the deposition rate and time. The IR measurement of the reference was performed using a Bruker Vertex 80v spectrometer combined with a liquid-N₂-cooled mercury cadmium telluride detector. The whole beam path was evacuated during the measurement. The spectrum was recorded with a resolution of 4 cm⁻¹ and 200 scans.

Micro-IR Spectroscopy. Infrared spectra were taken using IR radiation from the synchrotron light source SOLEIL. The measurements were performed with a ThermoFischer NICPLAN microscope coupled to a NEXUS 5700 spectrometer. The whole beam path coming from the synchrotron was purged with dry air. Light was detected using a liquid-N₂-cooled mercury cadmium telluride detector. The radiation provided by the synchrotron was already linearly polarized; therefore, all measurements were performed without the use of a polarizer. The measurements were normalized with respect to the bare CaF₂ substrate. In a first step, the antenna dimers were placed in the middle of a 15 μm × 15 μm knife edge aperture. To localize the highest IR response, systematic measurements of an area containing the dimer (6 × 6 points, 2 μm distance) were performed and the position with the best signal was used for the final measurements. All spectra were recorded with a resolution of 4 cm⁻¹ and at least 500 scans.

Numerical Simulations. Far-field extinction spectra and near-field distributions were calculated for a coverage of 5 nm CBP using the commercial FDTD software Lumerical FDTD Solutions v8.5.3. The optical data of gold were taken from Palik.⁴¹ The CaF₂ substrate was treated dispersionless with a constant refractive index of $n = 1.41$, and the dielectric function of CBP was taken from ref 28. Both the dielectric functions of gold and CBP were fitted with a built-in multi-coefficient model using 2 and 40 coefficients, respectively. Boundary conditions were defined by perfectly matched layers (PMLs) at least half a wavelength away from the structure. In order to reduce resources, the TFSF approach was chosen. To resolve the small gaps and the thin CBP layer, subgridding techniques were used: The mesh size

over the whole antenna was set to $1 \times 1 \times 1 \text{ nm}^3$, and the gap region was resolved with mesh sizes down to 0.5 nm for the smallest gap size. The default grid of the simulation region outside the nanostructures is defined by the auto-nonuniform mesh algorithm with a mesh accuracy of 5. The dimers were illuminated under normal incidence with a broadband (800–2000 cm⁻¹) plane wave polarized along the long antenna axis coming from the substrate direction. Electromagnetic field strengths were recorded with a 2D field profile monitor placed parallel to the substrate at half-height of the nanoantennas. The extinction cross section σ_{ext} was calculated by summing up the net power flowing inward through a rectangular box enclosing the nanoantenna dimer (absorbed light) and the power flowing outward through a rectangular box enclosing the TFSF source (scattered light), and then converted to a relative transmittance spectra by $T_{\text{rel}} = 1 - (\sigma_{\text{ext}}/A_0)$, where A_0 denotes the aperture size used in the respective experiment. The simulation time was set to 3000 fs. Such a long time was necessary because the CBP layer contains narrow band oscillators which leads to slowly decaying fields. To further reduce the computational resources, all symmetries provided by the structure were included in the simulation setup. All simulations were performed taking advantage of the high-performance cluster bwGRID.

Conflict of Interest: The authors declare no competing financial interest.

Acknowledgment. Financial support by the European project NANOANTENNA (HEALTH-F5-2009-241818) is gratefully acknowledged by the authors from the Kirchhoff-Institute for Physics and the Italian Institute of Technology. C.H. acknowledges financial support by the Helmholtz Graduate School for Hadron and Ion Research. C.H. and J.V. acknowledge financial support by the Heidelberg Graduate School of Fundamental Physics. J.K. and T.H. gratefully acknowledge the research training group "Nano- and biotechnologies for packaging of electronic devices" (DFG 1401) and the FhG Internal Programs (Grant No. Attract 692271) for funding. F.N. thanks the BW-Stiftung for financial support. We acknowledge SOLEIL for provision of synchrotron radiation facilities, and we would like to thank P. Dumas and F. Jamme for assistance in using beamline SMIS. We are grateful for computational resources provided by the bwGRID of the federal state of Baden-Wuerttemberg, Germany. The CBP deposition was done under the guidance of Tobias Glaser at the clustertool of the BMBF MESOMERIE Project (FKZ 13N10724) hosted by the InnovationLab GmbH, Heidelberg, Germany.

Supporting Information Available: Additional near-field maps, further information about the baseline correction, detuning correction, and estimation of C_{gap} . This material is available free of charge via the Internet at <http://pubs.acs.org>.

Note Added after ASAP Publication: After this paper was published ASAP on April 16, 2014, a correction was made to the description of CBP film evaporation and reference measurement in the Methods section. The corrected version was reposted April 22, 2014.

REFERENCES AND NOTES

- Bardhan, R.; Grady, N. K.; Cole, J. R.; Joshi, A.; Halas, N. J. Fluorescence Enhancement by Au Nanostructures: Nano-shells and Nanorods. *ACS Nano* **2009**, 3, 744–752.
- Kinkhabwala, A.; Yu, Z.; Fan, S.; Avlasevich, Y.; Mullen, K.; Moerner, W. E. Large Single-Molecule Fluorescence Enhancements Produced by a Bowtie Nanoantenna. *Nat. Photonics* **2009**, 3, 654–657.
- Aouani, H.; Šípová, H.; Rahmani, M.; Navarro-Cia, M.; Hegnerová, K.; Homola, J.; Hong, M.; Maier, S. A. Ultrasensitive Broadband Probing of Molecular Vibrational Modes with Multifrequency Optical Antennas. *ACS Nano* **2013**, 7, 669–675.
- Cataldo, S.; Zhao, J.; Neubrech, F.; Frank, B.; Zhang, C.; Braun, P. V.; Giessen, H. Hole-Mask Colloidal Nanolithography for Large-Area Low-Cost Metamaterials and Antenna-Assisted Surface-Enhanced Infrared Absorption Substrates. *ACS Nano* **2012**, 6, 979–985.

5. D'Andrea, C.; Bochterle, J.; Toma, A.; Huck, C.; Neubrech, F.; Messina, E.; Fazio, B.; Maragò, O. M.; Di Fabrizio, E.; Lamy de La Chapelle, M.; *et al.* Optical Nanoantennas for Multiband Surface-Enhanced Infrared and Raman Spectroscopy. *ACS Nano* **2013**, *7*, 3522–3531.
6. Kneipp, K.; Wang, Y.; Kneipp, H.; Perelman, L. T.; Itzkan, I.; Dasari, R. R.; Feld, M. S. Single Molecule Detection Using Surface-Enhanced Raman Scattering (SERS). *Phys. Rev. Lett.* **1997**, *78*, 1667–1670.
7. Theiss, J.; Pavaskar, P.; Echternach, P. M.; Muller, R. E.; Cronin, S. B. Plasmonic Nanoparticle Arrays with Nanometer Separation for High-Performance SERS Substrates. *Nano Lett.* **2010**, *10*, 2749–2754.
8. Nie, S.; Emory, S. R. Probing Single Molecules and Single Nanoparticles by Surface-Enhanced Raman Scattering. *Science* **1997**, *275*, 1102–1106.
9. Fazio, B.; D'Andrea, C.; Bonaccorso, F.; Irrera, A.; Calogero, G.; Vasi, C.; Gucciardi, P. G.; Allegrini, M.; Toma, A.; Chiappe, D.; *et al.* Re-radiation Enhancement in Polarized Surface-Enhanced Resonant Raman Scattering of Randomly Oriented Molecules on Self-Organized Gold Nanowires. *ACS Nano* **2011**, *5*, 5945–5956.
10. Neubrech, F.; Pucci, A.; Cornelius, T. W.; Karim, S.; Garcá-Etxarri, A.; Aizpurua, J. Resonant Plasmonic and Vibrational Coupling in a Tailored Nanoantenna for Infrared Detection. *Phys. Rev. Lett.* **2008**, *101*, 157403.
11. Adato, R.; Yanik, A. A.; Amsden, J. J.; Kaplan, D. L.; Omenetto, F. G.; Hong, M. K.; Erramilli, S.; Altug, H. Ultrasensitive Vibrational Spectroscopy of Protein Monolayers with Plasmonic Nanoantenna Arrays. *Proc. Natl. Acad. Sci. U.S.A.* **2009**, *106*, 19227–19232.
12. Weber, D.; Katzmann, J.; Neubrech, F.; Härtling, T.; Pucci, A. Spectral Tuning of IR-Resonant Nanoantennas by Nanogap Engineering. *Opt. Mater. Express* **2011**, *1*, 1301–1306.
13. Neubrech, F.; Weber, D.; Katzmann, J.; Huck, C.; Toma, A.; Di Fabrizio, E.; Pucci, A.; Härtling, T. Infrared Optical Properties of Nanoantenna Dimers with Photochemically Narrowed Gaps in the 5 nm Regime. *ACS Nano* **2012**, *6*, 7326–7332.
14. Alonso-González, P.; Albella, P.; Golmar, F.; Arzubiaga, L.; Casanova, F.; Hueso, L. E.; Aizpurua, J.; Hillenbrand, R. Visualizing the Near-Field Coupling and Interference of Bonding and Anti-bonding Modes in Infrared Dimer Nanoantennas. *Opt. Express* **2013**, *21*, 1270–1280.
15. Alonso-González, P.; Albella, P.; Schnell, M.; Chen, J.; Huth, F.; Garcia-Etxarri, A.; Casanova, F.; Golmar, F.; Arzubiaga, L.; Hueso, L.; *et al.* Resolving the Electromagnetic Mechanism of Surface-Enhanced Light Scattering at Single Hot Spots. *Nat. Commun.* **2012**, *3*, 684.
16. Aizpurua, J.; Bryant, G. W.; Richter, L. J.; Garcá de Abajo, F. J.; Kelley, B. K.; Mallouk, T. Optical Properties of Coupled Metallic Nanorods for Field-Enhanced Spectroscopy. *Phys. Rev. B* **2005**, *71*, 235420.
17. Dregely, D.; Neubrech, F.; Duan, H.; Vogelgesang, R.; Giessen, H. Vibrational Near-Field Mapping of Planar and Buried Three-Dimensional Plasmonic Nanostructures. *Nat. Commun.* **2013**, *4*, 2237.
18. Le Ru, E. C.; Grand, J.; Félidj, N.; Aubard, J.; Lévi, G.; Hohenau, A.; Krenn, J. R.; Blackie, E.; Etchegoin, P. G. Experimental Verification of the SERS Electromagnetic Model beyond the $|E|^4$ Approximation: Polarization Effects. *J. Phys. Chem. C* **2008**, *112*, 8117–8121.
19. Ru, E. L.; Etchegoin, P. Rigorous Justification of the $|E|^4$ Enhancement Factor in Surface Enhanced Raman Spectroscopy. *Chem. Phys. Lett.* **2006**, *423*, 63–66.
20. Sawai, Y.; Takimoto, B.; Nabika, H.; Ajito, K.; Murakoshi, K. Observation of a Small Number of Molecules at a Metal Nanogap Arrayed on a Solid Surface Using Surface-Enhanced Raman Scattering. *J. Am. Chem. Soc.* **2007**, *129*, 1658–1662.
21. Duan, H.; Hu, H.; Kumar, K.; Shen, Z.; Yang, J. K. W. Direct and Reliable Patterning of Plasmonic Nanostructures with Sub-10-nm Gaps. *ACS Nano* **2011**, *5*, 7593–7600.
22. Wang, H.; Levin, C. S.; Halas, N. J. Nanosphere Arrays with Controlled Sub-10-nm Gaps as Surface-Enhanced Raman Spectroscopy Substrates. *J. Am. Chem. Soc.* **2005**, *127*, 14992–14993.
23. Hatab, N. A.; Hsueh, C.-H.; Gaddis, A. L.; Rettner, S. T.; Li, J.-H.; Eres, G.; Zhang, Z.; Gu, B. Free-Standing Optical Gold Bowtie Nanoantenna with Variable Gap Size for Enhanced Raman Spectroscopy. *Nano Lett.* **2010**, *10*, 4952–4955.
24. Käll, M.; Xu, H.; Johansson, P. Field Enhancement and Molecular Response in Surface-Enhanced Raman Scattering and Fluorescence Spectroscopy. *J. Raman Spectrosc.* **2005**, *36*, 510–514.
25. Tian, J.-H.; Liu, B.; Xiulan; Yang, Z.-L.; Ren, B.; Wu, S.-T.; Tao, Tian, Z.-Q. Study of Molecular Junctions with a Combined Surface-Enhanced Raman and Mechanically Controllable Break Junction Method. *J. Am. Chem. Soc.* **2006**, *128*, 14748–14749.
26. Pucci, A.; Neubrech, F.; Weber, D.; Hong, S.; Toury, T.; de la Chapelle, M. L. Surface Enhanced Infrared Spectroscopy Using Gold Nanoantennas. *Phys. Status Solidi B* **2010**, *247*, 2071–2074.
27. Han, G.; Weber, D.; Neubrech, F.; Yamada, I.; Mitome, M.; Bando, Y.; Pucci, A.; Nagao, T. Infrared Spectroscopic and Electron Microscopic Characterization of Gold Nanogap Structure Fabricated by Focused Ion Beam. *Nanotechnology* **2011**, *22*, 275202.
28. Glaser, T.; Beck, S.; Lunkhenheimer, B.; Donhauser, D.; Köhn, A.; Kröger, M.; Pucci, A. Infrared Study of the MoO_3 Doping Efficiency in 4,4'-Bis(*N*-carbazolyl)-1,1'-biphenyl (CBP). *Org. Electron.* **2013**, *14*, 575–583.
29. Weber, D.; Albella, P.; Alonso-González, P.; Neubrech, F.; Gui, H.; Nagao, T.; Hillenbrand, R.; Aizpurua, J.; Pucci, A. Longitudinal and Transverse Coupling in Infrared Gold Nanoantenna Arrays: Long Range *versus* Short Range Interaction Regimes. *Opt. Express* **2011**, *19*, 15047–15061.
30. Giannini, V.; Francescato, Y.; Amrania, H.; Phillips, C. C.; Maier, S. A. Fano Resonances in Nanoscale Plasmonic Systems: A Parameter-Free Modeling Approach. *Nano Lett.* **2011**, *11*, 2835–2840.
31. Neubrech, F.; Pucci, A. Plasmonic Enhancement of Vibrational Excitations in the Infrared. *IEEE J. Sel. Top. Quantum Electron.* **2013**, *19*, 4600809.
32. Ross, B. M.; Lee, L. P. Comparison of near- and Far-Field Measures for Plasmon Resonance of Metallic Nanoparticles. *Opt. Lett.* **2009**, *34*, 896–898.
33. Zuloaga, J.; Nordlander, P. On the Energy Shift between Near-Field and Far-Field Peak Intensities in Localized Plasmon Systems. *Nano Lett.* **2011**, *11*, 1280–1283.
34. Alonso-González, P.; Albella, P.; Neubrech, F.; Huck, C.; Chen, J.; Golmar, F.; Casanova, F.; Hueso, L. E.; Pucci, A.; Aizpurua, J.; *et al.* Experimental Verification of the Spectral Shift between Near- and Far-Field Peak Intensities of Plasmonic Infrared Nanoantennas. *Phys. Rev. Lett.* **2013**, *110*, 203902.
35. Kern, A. M.; Martin, O. J. F. Excitation and Reemission of Molecules near Realistic Plasmonic Nanostructures. *Nano Lett.* **2011**, *11*, 482–487.
36. Esteban, R.; Borisov, A. G.; Nordlander, P.; Aizpurua, J. Bridging Quantum and Classical Plasmonics with a Quantum-Corrected Model. *Nat. Commun.* **2012**, *3*, 825.
37. Eilers, P. H. C. A Perfect Smoother. *Anal. Chem.* **2003**, *75*, 3631–3636.
38. Brown, L. V.; Zhao, K.; King, N.; Sobhani, H.; Nordlander, P.; Halas, N. J. Surface-Enhanced Infrared Absorption Using Individual Cross Antennas Tailored to Chemical Moieties. *J. Am. Chem. Soc.* **2013**, *135*, 3688–3695.
39. Horodecki, M.; Oppenheim, J. Fundamental Limitations for Quantum and Nanoscale Thermodynamics. *Nat. Commun.* **2013**, *4*, 2059.
40. Scout, version 3.62; Theiss, W. Hard- and Software, Aachen, Germany, 2012.
41. Palik, E. D. *Handbook of Optical Constants of Solids*; Academic Press: New York, 1985.